

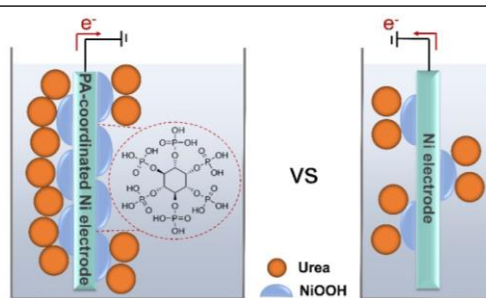
Phytate-Coordination Triggered Enrichment of Surface NiOOH Species on Nickel Foam for Efficient Urea Electrooxidation

Jiayuan Li^{1#}, Yuefei Li^{1#}, Qingyu Xue¹, Yuchi Gao¹ and Yuanyuan Ma¹

¹Key Laboratory of Special Functional and Smart Polymer Materials of Ministry of Industry and Information Technology, School of Chemistry and Chemical Engineering, Northwestern Polytechnical University, Xi'an 710072, China

ABSTRACT Nickel (Ni)-based materials are promising electrocatalysts for the urea electrooxidation reaction, as the *in situ* formed NiOOH species on their surface during operation are catalytically active sites. In this work, phytate-coordinated Ni foam (PA-NF) is shown to deliver a high catalytic performance, with a potential as low as 1.38 V at 10 mA/cm², a Tafel slope as low as 64.1 mV/dec, and superior catalytic stability. Characterizations revealed that such a high performance was ascribed to the kinetic acceleration of surface reconstruction and the enriched NiOOH active species on the PA-NF surface owing to PA-coordination induced upshift of d-band center of Ni sites. Overall, a novel and simple strategy is provided for designing the efficient as well as universal Ni-based catalyst for the electrooxidation of urea, which can also be extended to other transition-metal-based systems.

Keywords: phytates, surface coordination, urea electrooxidation reaction, electrocatalysis



INTRODUCTION

The electrocatalytic urea oxidation reaction (UOR) in basic electrolyte is crucial for direct urea/urine fuel cells, urea-rich wastewater treatment, and urea-boosted water electrolysis.^[1-4] Thus, the research on UOR has important implications for energy and environment fields. Considering the 6 electron transfer number for UOR, this reaction experiences sluggish kinetics, therefore making it necessary to develop electrocatalysts that have strong affinity toward urea to accelerate the reaction kinetics while suppressing the 4e⁻ oxygen evolution reaction (OER).^[5,6]

Nickel (Ni)-based materials can be used for the electrooxidation of urea as they undergo surface reconstruction and form NiOOH as an active species, with the electrophilic OH^{*} groups of NiOOH interacting with urea.^[7] Thus, a great amount of focus has been placed on designing Ni-based catalysts with in-situ formed NiOOH for urea electrooxidation.^[7,8] However, the catalytic activity of current Ni-based catalysts is still insufficient because their surface reconstruction process is still uncontrollable and inefficient.^[9] Thus, it is highly desirable to develop a strategy for controlling this surface reconstruction process to enrich the surface NiOOH species during the electrooxidation of urea.

In this work, the Ni foam (NF) is selected as a model catalyst. The utilization of phytate (PA)-coordination on NF via the simply hydrothermal reaction between NF and PA in aqueous solution is proposed. Using this strategy, the resulting PA-NF electrode delivers a high catalytic activity for electrocatalytic urea oxidation, with a potential as low as 1.38 V at 10 mA/cm², a Tafel slope as low as 64.1 mV/dec, and excellent catalytic stability. Electrochemical investigations and control experiments confirmed accelerated reconstruction of the catalyst and the concentration of the PA-NF electrode surface with NiOOH active species during the electrooxidation of urea owing to PA-coordination induced regu-

lation of d-band center of Ni sites, thus improving the overall catalytic activity.

RESULTS AND DISCUSSION

PA-NF electrode samples were synthesized via the facile hydrothermal reaction between clean NF and phytic acid at 120 °C (Figure 1a). Its fourier-transform infrared (FT-IR) spectrum (Figure 1b) shows the FT-IR peaks at 1639, 1387, 1055, and 558 cm⁻¹, attributed to the stretching of P=O, phosphate, symmetrical P-O-C, and P-O-H, respectively, thus confirming the successful synthesis of the electrode.^[10] The strong consistency between the peaks present in the FT-IR signal of both PA-NF and pristine PA supports the existence of PA on NF surface (Figure S1). The X-ray diffraction (XRD), scanning electron microscopy (SEM) and energy-dispersive X-ray (EDX) elemental mapping results further suggest the uniform distribution of P element in PA on the surface of NF as well as the good preservation of the Ni bulk phase after the coordination of PA on the surface of the NF (Figures 1c-d and S2). In the X-ray photoelectron spectroscopy (XPS) profiles, apparent Ni and P can be noticed (Figure 1e-f). In the Ni 2p_{3/2} region, a dominant peak for the Ni⁰ species of pristine NF can be observed at 852.5 eV, while an obvious peak for the Ni²⁺ species of PA-NF appears at 855.9 eV (Figure 1d). Such phenomena are owing to the PA coordination on NF and thereby the Ni-to-PA charge transfer.^[11-14] The Ni²⁺ species can also be found for bare NF due to its surface oxidation in ambient conditions.^[15] In the P 2p region (Figure 1f), an apparent peak at 133.9 eV is indexed to the PO_x species,^[16] again supporting the PA coordination on NF surface.

Then, we investigated the catalytic activity of the as-prepared electrodes for the electrooxidation of urea. Figure 2a shows the linear sweep voltammetry (LSV) profiles of pristine NF and PA-NF in the presence (0.33 M) or absence of urea in a three-electrode

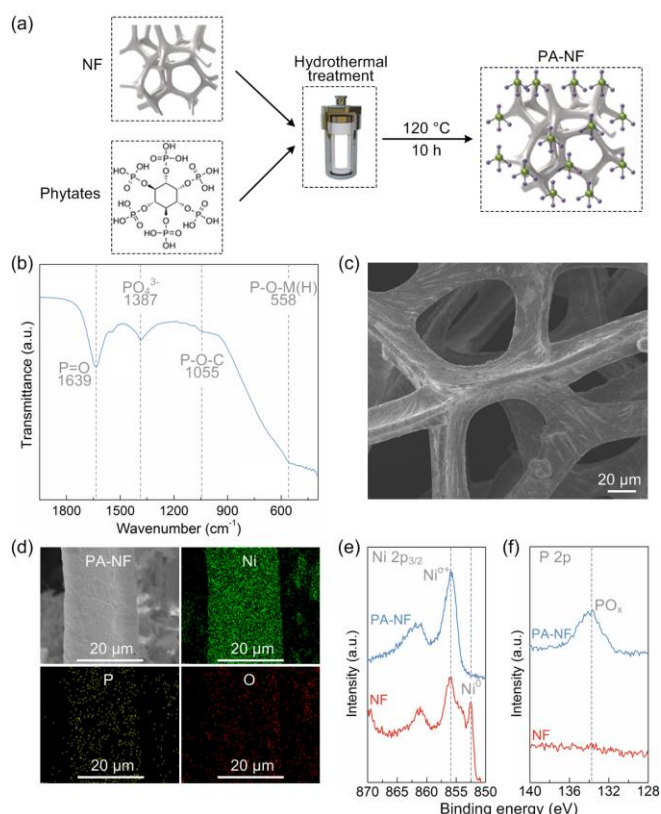


Figure 1. (a) The schematic diagram for the synthesis of PA-NF. (b) FT-IR spectrum of PA-NF. (c) SEM image and (d) EDX elemental mapping of PA-NF. High-resolution XPS spectra of PA-NF and NF in (e) Ni 2p_{3/2} and (f) P 2p region.

system containing 1.0 M KOH solution. With the addition of urea, the NF electrode displayed an almost unchanged potential at 10 mA/cm² (E_{10} = 1.47 V). In comparison, the PA-NF electrode delivered a significantly decreased E_{10} value (1.38 V). The sharp decrement of Tafel slope for PA-NF (64.1 mV/dec) compared with that of NF (145.2 mV/dec) reflects its accelerated catalytic kinetics toward the electrooxidation of urea. Overall, the catalytic activity of PA-NF was found to be better than that of the NF and comparable to those of state-of-the-art Ni-based catalysts (Figure 2b and Table S1). It is thus confirmed that PA coordination plays a crucial role in the significant enhancement in the activity of the electrode toward the UOR. Moreover, the PA-NF electrode displayed catalytic stability for at least 40 h (Figure 2c). The high similarity of the XPS profiles in P 2p region for the fresh and spent PA-NF excluded the oxidation of PA molecules after long-term operation (Figure S3). With the inductively coupled plasma mass spectrometry (ICP-MS) investigations on the electrolyte after long-term catalysis, trace amounts of metal ions (1.0 ppm) were leached in the given (40 mL) electrolyte (Table S2). All of the above results suggest the catalytic robustness of the PA-NF electrode and its potential for practical applications.

Next, the role that the coordination of PA plays was examined. Generally, the NiOOH species on the surface of the Ni-based catalysts should form and then subsequently react with urea in

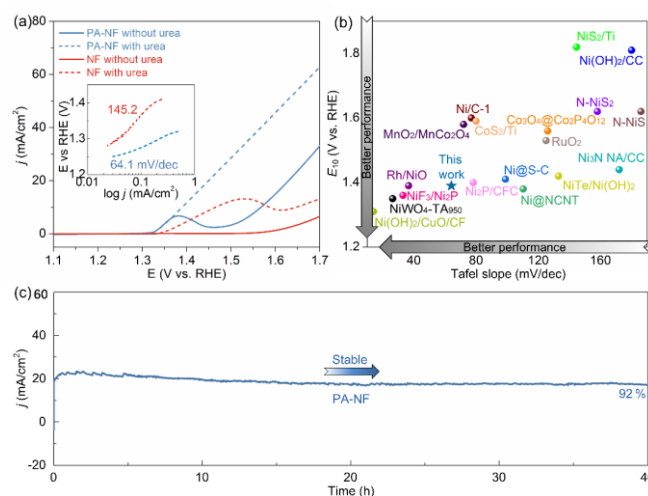


Figure 2. (a) LSV curves of PA-NF and NF in the presence and absence of urea (0.33 M), measured in 1.0 M KOH electrolyte at a scan rate of 10 mV/s. Inset shows the corresponding Tafel plots of the PA-NF and NF electrodes. (b) Comparison of the catalytic performance of the PA-NF electrode with those of state-of-the-art Ni-based UOR electrocatalysts derived from Table S1. (c) Catalytic durability over the PA-NF electrode at a constant potential of 1.45 V vs. RHE with continuous supply of urea.

electrocatalytic urea oxidation.^[7] Thus, it is likely that the coordination of PA to NF facilitates NiOOH generation. To examine this, the reconstruction of surface species on the PA-NF and NF electrodes during the electrooxidation of urea was evaluated using Raman technology. When urea is present in electrolyte, the spent PA-NF and NF showed no peaks in their Raman spectra (Figure S4), while when the electrolyte did not contain urea, two apparent peaks at 478.7 and 560.8 cm⁻¹ were observed in the Raman spectra of the spent PA-NF and NF (Figure S5), which is indexed to the Ni-O vibrations of NiOOH.^[17] Afterwards, the XPS investigations on the spent PA-NF and NF electrodes displayed a stronger peak at 857.0 eV in the Ni 2p_{3/2} region (Figure S6), indexed to the Ni³⁺ in NiOOH.^[18] The above results strongly supported that the in-situ generation and consumption of NiOOH catalytic species dominated the electrooxidation of urea for both PA-NF and NF,^[19–22] thus enabling a straight-forward examination of the roles that PA plays in the reconstruction of the surface of electrode, the formation of NiOOH active species and the influence that it has on the catalytic performance of the electrode in the electro oxidation of urea.

To further examine the reconstruction of the surface of the PA-NF electrode, cyclic voltammetry (CV) experiments were conducted over the NF and PA-NF (Figure 3a). For NF electrode, a Ni²⁺/Ni³⁺ redox peak was observed at 1.43 V vs. RHE. In comparison, the significantly lower Ni²⁺/Ni³⁺ redox potential at 1.39 V vs. RHE for the PA-NF electrode strongly implied reconstruction of the surface of the electrode and the formation of NiOOH more readily occurring after the coordination of PA.^[23] Then, the in-situ formed NiOOH was calculated by integrating the j vs. E of the CV curves. Clearly, the integrated value of the PA-NF electrode was 33 times higher than that of the NF electrode, suggesting that

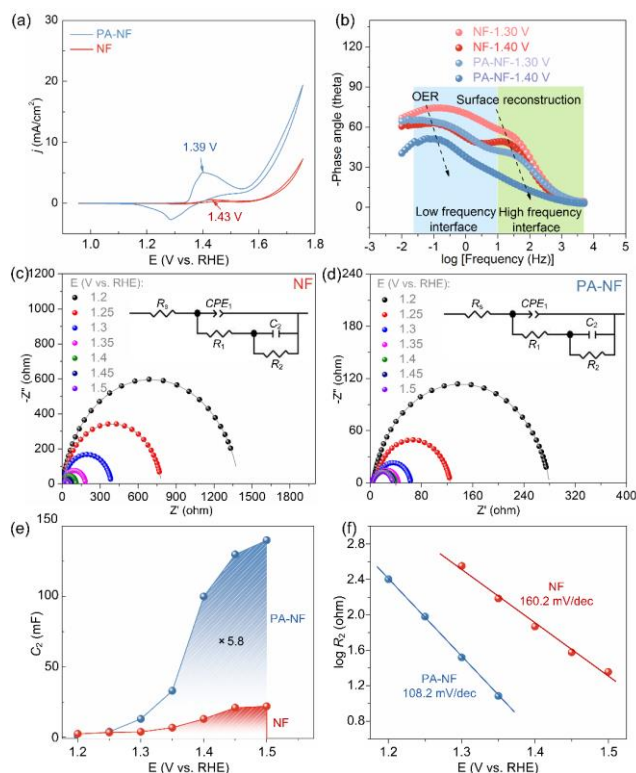


Figure 3. (a) CV curves of the PA-NF and NF electrodes in 1.0 M KOH electrolyte. (b) Bode plots of the NF and PA-NF electrodes at various potentials. Nyquist plots for (c) NF and (d) PA-NF electrodes at various potentials. The scattered symbols represent the experimental results, and the solid lines are simulated fitting results. The inset also shows the equivalent circuit for the simulation. The fitted parameters are summarized in Table S3. (e) Plots of C_2 vs. E of the NF and PA-NF electrodes during the reconstruction of their surfaces. (f) EIS-derived Tafel plots of the NF and PA-NF electrodes obtained from the surface reconstruction resistance, R_2 .

accelerated reconstruction of the electrode surface and the concentration of the surface with NiOOH active species occurred during the reaction owing to the coordination of PA.

Then, the electrochemical impedance spectra (EIS) were recorded within the potential ranging from 1.3–1.4 V vs. RHE to investigate the process of the reconstruction of the surfaces of the PA-NF and NF electrodes.^[19] Generally, the high-frequency region in the Bode plots represents the surface reconstruction behavior of electrodes.^[24] Herein, the significantly smaller phase angle of the PA-NF electrode in comparison with that of the NF electrode at each potential (Figure 3b) is strong evidence of the significant acceleration of surface reconstruction and concentration of NiOOH active species that take place on the PA-coordinated NF electrode.^[24] Besides this, the Nyquist plots of the PA-NF and NF electrodes were fitted using a double-parallel equivalent circuit model (Figure 3c–3d and Table S3). The first parallel components (CPE_1 and R_1) reflect the charge-transfer kinetics.^[25] Small values of R_1 for all the catalysts suggested their good conductivity and thereby fast charge-transfer kinetics for UOR.

The second parallel components (C_2 and R_2) represent the pseudo-capacitance and resistance of the reconstruction of the surfaces of the electrodes, respectively.^[24] As shown in Figure 3e, the integrated profiles of C_2 vs. E provide information on the charge that is generated during the reconstruction of the surfaces of the electrodes.^[24,26,27] The charge of the PA-NF electrode was 5.8 times higher than that of the NF electrode, implying the concentration of the PA-NF electrode with NiOOH active species via the reconstruction of its surface.

The electrochemically surface area (ECSA) of various electrodes was determined by CV curves with various scan rates (Figure S7) to calculate the double layer capacitance (C_{dl}). As shown in Figure S8, C_{dl} values of PA-NF and NF were found to be 41.2 and 5.9 mF. Then, the ECSA of various electrodes was estimated by $ECSA = C_{dl}/C_s$, where C_s is the specific capacitance of the sample or the capacitance of an atomically smooth planar surface of the material per unit area under identical electrolyte conditions. For our estimates of ECSA, we use general $C_s = 0.04$ mF/cm² in 1.0 M NaOH based on typical reported values.^[28] Thus, the calculated ECSA was presented in Table S4. Afterwards, the normalized polarization curves for UOR of various electrodes are shown in Figure S9. The NF showed higher intrinsic activity for UOR compared with that of PA-NF, further demonstrating the enhanced overall UOR performance of PA-NF owing to the acceleration of surface reconstruction and concentration of NiOOH species.

Considering that R_2 is potential-dependent for both types of electrodes, the relationship between $\log R_2$ and the potentials/EIS-calculated Tafel slopes could be used to quantify the kinetics of the reconstruction of the surfaces of the electrodes.^[25] As shown in Figure 3f, the faster kinetics involved in the reconstruction of the surface of PA-NF electrode are reflected by its lower Tafel slope (108.2 mV/dec) compared to that of NF (160.2 mV/dec) electrode. This demonstrates the greatly facilitated surface reconstruction and NiOOH active species generation on a PA-NF electrode during UOR owing to the PA coordination.

During UOR, the surface reconstruction and generation of NiOOH catalytic species of Ni-based electrodes is an oxidation process starting from Ni sites, which highly depends on the adsorbed intermediates (such as OH_{ads} , O_{ads} and OOH_{ads}).^[29–31] In fact, the d-band centers of PA-NF and NF measured from their valence band spectra were -2.51 and -3.05 eV respectively (Figure 4), which clearly demonstrated that the d-band center

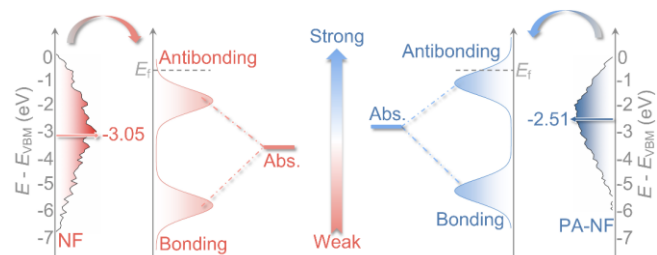


Figure 4. High-resolution valence band profiles of Ni relative to the valence band maximum (VBM) for the NF and PA-NF electrodes. Such profiles in the range from 0 to -10.0 eV serve as an analogue of the density of states. Arrows indicate the positions of the d-band centers.

shifted closer to the E_f of Ni sites after PA coordination. According to the d-band center theory, these findings suggest that more antibonding electronic states of PA-NF are filled and the interaction between the abovementioned intermediates and Ni sites with PA coordination is strengthened during UOR,^[32] thus inducing the accelerated surface reconstruction and NiOOH active species concentration on PA-NF electrode during UOR. Overall, PA coordination could regulate the d-band centers of Ni sites and bring the acceleration of surface reconstruction as well as concentration of NiOOH active species during UOR, eventually enhancing the overall catalytic performance.

CONCLUSION

In summary, Ni foam electrodes featuring phytate coordination have been demonstrated to effectively deliver high catalytic performance toward urea electrooxidation with a low potential, a low Tafel slope, and robust durability. Electrochemical investigations alongside control experiments unambiguously illustrated accelerated surface reconstruction and the concentration of the surface of Ni foam with NiOOH active species due to phytate-coordination induced upshift of d-band center of Ni sites. This work thus provides a novel and simple strategy for manipulating the surface reconstruction of Ni-based materials during electrocatalytic oxidation reactions.

ACKNOWLEDGEMENTS

We acknowledge the financial support from the National Natural Science Foundation of Shaanxi province, China (2019JQ-486), the Young Talent Support Project of Shaanxi (20200601), and the Fundamental Research Funds for the Central Universities (No. D5000210651).

AUTHOR CONTRIBUTION

These authors contributed equally to this work.

AUTHOR INFORMATION

Corresponding author. Email: Jiayuanli@nwpu.edu.cn

COMPETING INTERESTS

The authors declare no competing interests.

ADDITIONAL INFORMATION

Supplementary information is available for this paper at <http://manu30.magtech.com.cn/jghx/EN/10.14102/j.cnki.0254-5861.2022-0095>

For submission: <https://mc03.manuscriptcentral.com/cjsc>

REFERENCES

- (1) Ke, K.; Wang, G.; Cao, D.; Wang, G. Recent advances in the electro-oxidation of urea for direct urea fuel cell and urea electrolysis. *Electrocatalysis* **2020**, 41-78.
- (2) Yao, S.; Wolfson, S.; Ahn, B.; Liu, C. Anodic oxidation of urea and an electrochemical approach to deureation. *Nature* **1973**, 241, 471-472.
- (3) Sayed, E. T.; Eisa, T.; Mohamed, H. O.; Abdelkareem, M. A.; Allagui, A.; Alawadhi, H.; Chae, K.-J. Direct urea fuel cells: challenges and opportunities. *J. Power Sources* **2019**, 417, 159-175.
- (4) Geng, S.-K.; Zheng, Y.; Li, S.-Q.; Su, H.; Zhao, X.; Hu, J.; Shu, H.-B.; Jaroniec, M.; Chen, P.; Liu, Q.-H. Nickel ferrocyanide as a high-performance urea oxidation electrocatalyst. *Nat. Energy* **2021**, 6, 904-912.
- (5) Senthilkumar, N.; Gnana Kumar, G.; Manthiram, A. 3D hierarchical core-shell nanostructured arrays on carbon fibers as catalysts for direct urea fuel cells. *Adv. Energy Mater.* **2018**, 8, 1702207.
- (6) Singh, R. K.; Rajavelu, K.; Montag, M.; Schechter, A. Advances in catalytic electrooxidation of urea: a review. *Energy Technol.* **2021**, 9, 2100017.
- (7) Chen, W.; Xie, C.; Wang, Y.; Zou, Y.; Dong, C.-L.; Huang, Y.-C.; Xiao, Z.; Wei, Z.; Du, S.; Chen, C. Activity origins and design principles of nickel-based catalysts for nucleophile electrooxidation. *Chem.* **2020**, 6, 2974-2993.
- (8) Hu, X.; Zhu, J.; Li, J.; Wu, Q. Urea electrooxidation: current development and understanding of Ni-based catalysts. *ChemElectroChem* **2020**, 7, 3211-3228.
- (9) Zhu, B.; Liang, Z.; Zou, R. Designing advanced catalysts for energy conversion based on urea oxidation reaction. *Small* **2020**, 16, 1906133.
- (10) Feng, X.; Xiao, Y.; Huang, H. H.; Wang, Q.; Wu, J.; Ke, Z.; Tong, Y.; Zhang, J. Phytic acid-based FeCo bimetallic metal-organic gels for electrocatalytic oxygen evolution reaction. *Chem. Asian J.* **2021**, 16, 3213-3220.
- (11) Chen, X.; Li, P.; Jin, Z.; Meng, Y.; Yuan, H.; Xiao, D. Tri-metallic phytate in situ electrodeposited on 3D Ni foam as a highly efficient electrocatalyst for enhanced overall water splitting. *J. Mater. Chem. A* **2017**, 5, 18786-18792.
- (12) Li, P. Y.; Hong, W. T.; Liu, W. Fabrication of large scale self-supported WC/Ni(OH)₂ electrode for high-current-density hydrogen evolution. *Chin. J. Struct. Chem.* **2021**, 40, 1365-1371.
- (13) Wu, Y. L.; Xie, N.; Li, X. F.; Fu, Z. M.; Wu, X. T.; Zhu, Q. L. MOF-derived hierarchical hollow NiRu-C nanohybrid for efficient hydrogen evolution reaction. *Chin. J. Struct. Chem.* **2021**, 40, 1346-1356.
- (14) Wu, H. S.; Miao, T. F.; Shi, H. X.; Xu, Y.; Fu, X. L.; Qian, L. Probing photocatalytic hydrogen evolution of cobalt complexes: experimental and theoretical methods. *Chin. J. Struct. Chem.* **2021**, 40, 1696-1709.
- (15) Grdeń, M.; Alsabet, M.; Jerkiewicz, G. Surface science and electro-chemical analysis of nickel foams. *ACS Appl. Mater. Inter.* **2012**, 4, 3012-3021.
- (16) Zhang, J.; Zhao, Z.; Xia, Z.; Dai, L. A metal-free bifunctional electrocatalyst for oxygen reduction and oxygen evolution reactions. *Nat. Nanotechnol.* **2015**, 10, 444-452.
- (17) Wang, H.; Li, C.; An, J.; Zhuang, Y.; Tao, S. Surface reconstruction of NiCoP for enhanced biomass upgrading. *J. Mater. Chem. A* **2021**, 9, 18421-18430.
- (18) Hao, P.; Xin, Y.; Wang, Q.; Li, L.; Zhao, Z.; Wen, H.; Xie, J.; Cui, G.; Tang, B. Lanthanum-incorporated β -Ni(OH)₂ nanoarrays for robust urea electro-oxidation. *Chem. Commun.* **2021**, 57, 2029-2032.
- (19) Huang, C.; Huang, Y.; Liu, C.; Yu, Y.; Zhang, B. Integrating hydrogen production with aqueous selective semi-dehydrogenation of tetrahydroisoquinolines over a Ni₂P bifunctional electrode. *Angew. Chem. Int. Ed.* **2019**, 58, 12014-12017.
- (20) Sun, H.; Zhang, W.; Li, J.-G.; Li, Z.; Ao, X.; Xue, K.-H.; Ostrikov, K. K.; Tang, J.; Wang, C. Rh-engineered ultrathin NiFe-LDH nanosheets enable highly-efficient overall water splitting and urea electrolysis. *Appl. Catal. B-Environ.* **2021**, 284, 119740.
- (21) Sun, H.; Tung, C.-W.; Qiu, Y.; Zhang, W.; Wang, Q.; Li, Z.; Tang, J.;

- Chen, H.-C.; Wang, C.; Chen, H. M. Atomic metal-support interaction enables reconstruction-free dual-site electrocatalyst. *J. Am. Chem. Soc.* **2022**, 144, 1174-1186.
- (22) Sun, H.; Yang, J.-M.; Li, J.-G.; Li, Z.; Ao, X.; Liu, Y.-Z.; Zhang, Y.; Li, Y.; Wang, C.; Tang, J. Synergistic coupling of NiTe nanoarrays with RuO₂ and NiFe-LDH layers for high-efficiency electrochemical-/photovoltage-driven overall water splitting. *Appl. Catal. B-Environ.* **2020**, 272, 118988.
- (23) Zhang, J.; Yu, P.; Zeng, G.; Bao, F.; Yuan, Y.; Huang, H. Boosting HMF oxidation performance via decorating ultrathin nickel hydroxide nanosheets with amorphous copper hydroxide islands. *J. Mater. Chem. A* **2021**, 9, 9685-9691.
- (24) Zhou, B.; Li, Y.; Zou, Y.; Chen, W.; Zhou, W.; Song, M.; Wu, Y.; Lu, Y.; Liu, J.; Wang, Y. Platinum modulates redox properties and 5-hydroxymethylfurfural adsorption kinetics of Ni(OH)₂ for biomass upgrading. *Angew. Chem. Int. Ed.* **2021**, 60, 22908-22914.
- (25) Damian, A.; Omanovic, S. Ni and NiMo hydrogen evolution electrocatalysts electrodeposited in a polyaniline matrix. *J. Power Sources* **2006**, 158, 464-476.
- (26) Šimpraga, R.; Tremiliosi-Filho, G.; Qian, S.; Conway, B. In situ determination of the 'real area factor' in H₂ evolution electrocatalysis at porous Ni-Fe composite electrodes. *J. Electroanal. Chem.* **1997**, 424, 141-151.
- (27) Bai, L.; Harrington, D.; Conway, B. Behavior of overpotential—deposited species in faradaic reactions—II. ac Impedance measure-

- ments on H₂ evolution kinetics at activated and unactivated Pt cathodes. *Electrochim. Acta* **1987**, 32, 1713-1731.
- (28) McCrory, C. C.; Jung, S.; Peters, J. C.; Jaramillo, T. F. Benchmarking heterogeneous electrocatalysts for the oxygen evolution reaction. *J. Am. Chem. Soc.* **2013**, 135, 16977-16987.
- (29) Garcia, A. C.; Touzalin, T.; Nieuwland, C.; Perini, N.; Koper, M. T. Enhancement of oxygen evolution activity of nickel oxyhydroxide by electrolyte alkali cations. *Angew. Chem. Int. Ed.* **2019**, 58, 12999-13003.
- (30) Michael, J. D.; Demeter, E. L.; Illes, S. M.; Fan, Q.; Boes, J. R.; Kitchin, J. R. Alkaline electrolyte and Fe impurity effects on the performance and active-phase structure of NiOOH thin films for OER catalysis applications. *J. Phys. Chem. C* **2015**, 119, 11475-11481.
- (31) Diaz-Morales, O.; Ferrus-Suspedra, D.; Koper, M. T. The importance of nickel oxyhydroxide deprotonation on its activity towards electrochemical water oxidation. *Chem.Sci.* **2016**, 7, 2639-2645.
- (32) Nørskov, J. K.; Abild-Pedersen, F.; Studt, F.; Bligaard, T. Density functional theory in surface chemistry and catalysis. *Proc. Natl. Acad. Sci.* **2011**, 108, 937-943.

Received: May 6, 2022

Accepted: May 22, 2022

Published online: May 26, 2022

Published: July 18, 2022